MALAYSIAN JOURNAL OF SCIENCE
MJS
ISSN 1394 - 3065

5th International Conference on Applied & Industrial Mathematics and Statistics 2025 (ICoAIMS 2025)

Special Issue

Malaysian Journal of Science 45 (Special Issue 2): 74-82 (November 2026) https://mjs.um.edu.my

Numerical Computation of Second Rank Polarization Tensor with Speeding Up Techniques

Suzarina Ahmed Sukri[1a*], Yeak Su Hoe[2a], Taufiq Khairi Ahmad Khairuddin[3a] and Nurfarrisha Asnida Khairul Akmar[4a]

Abstract: This research focused on the techniques used to accelerate the numerical computation of the second rank polarization tensor (PT), which plays a crucial part in many real-life applications such as mathematics and engineering. In order to achieve an accurate numerical solution of PT with reduced computation time, this study employed a different yet simple technique for handling the higher singularity in the mathematical computation of PT itself. By leveraging numerical integration techniques together with the adaptive mesh refinement technique, it shows that the computation of the numerical solution can be achieved within a shorter time without sacrificing accuracy. From the results, a lower computational time is achieved with a higher precision numerical solution, making these techniques practical in complex systems, especially in engineering applications. This research not only improves computational speed but also enhances efficiency and accuracy by implementing adaptive geometrical modifications with the aids of meshing tool which is Netgen Mesh Generator.

Keywords: Polarization tensor, numerical integration, adaptive mesh refinement, computational efficiency

1. Introduction

The polarization tensor (PT) has attracted considerable attention from researchers, particularly in engineering and science. In this context, the term "tensor" originates from the field of mathematics, where it is used to describe the characteristics of objects that may vary according to their directions. This phenomenon appears in several real-life problems, for example, in the properties of crystalline substances, where these properties differ but correspond to their directions. In this case, we describe it as anisotropic. A researcher named Polya represented PT as an induced mass of an object for which objects with no conductivity move in a fluid (Polya, 1947). The second rank PT contains both physical and geometrical properties of an object. In subsequent years, PT has been further developed, where, instead of PT, researchers derived the mathematical formulation of PT and called it the Generalized Polarization Tensor (GPT). GPT is expressed as an asymptotic formula, where the dominant terms in that formula are referred to as the second rank PT (SRPT) or the first order PT (FPT). Since PT contains information regarding object inclusion, these characteristics make it useful for distinguishing between utilized and non-utilized objects. Overall, the concept of GPT, introduced by Polya and Szego, has significantly expanded the original version of PT pioneered by Polya. This concept has been widely employed by other researchers in the same field, as seen in Ammari and Kang (2007), Friedman and Vogelius (1989), de Jong et al. (2000), and Polya (1997). The application of PT can be seen in many areas, including electrosensing, medical imaging, electrical imaging, metal detection, and many other uses (Ammari & Kang, 2003, 2006, 2007; Bardet & Vasseur, 2005; Bannister & Gupta, 2009; Roux & Gloaguen, 2016; Alkhalifah, 2014). For instance, PT was used in a model of electrical impedance tomography (EIT), where the system is employed by an engineer to measure voltages on the surface of a body, which can determine the image of objects that might appear inside human bodies (Ammari & Kang, 2007). Meanwhile, breast anomalies detected by T-scan detection are demonstrated by Ammari and Kang (2003), where PT was employed in mathematical modeling of the anomaly's image, as illustrated in Figure 1(a), where the breast abnormality is reconstructed using the model of PT.

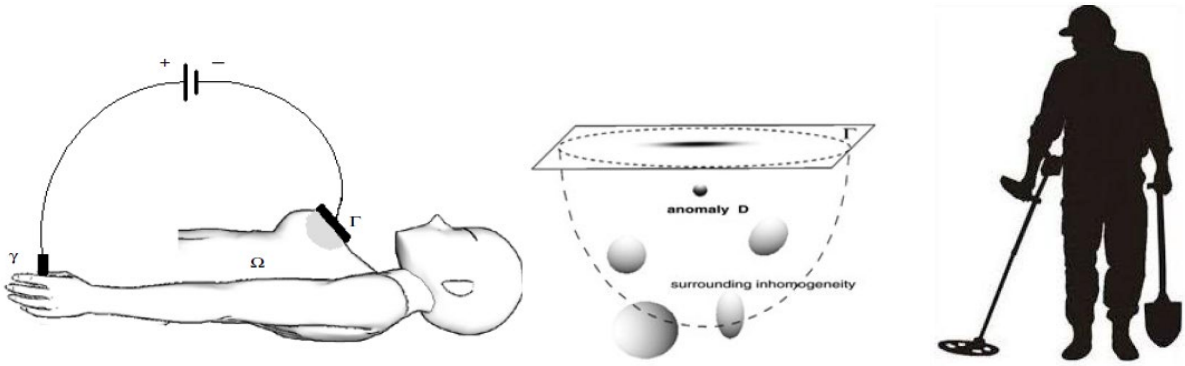
The computation of the second rank PT is crucial in various applications where it requires accuracy to ensure no false results are obtained. For example, in metal detection, we can differentiate between metallic and non-metallic objects, which necessitates the use of highly accurate methods. The inaccuracy of these numerical results can lead to unreliable numerical techniques, which may cause high costs in real-life problems. Previously, several numerical methods were developed to compute SRPT for various geometries, such as the Boundary Element Method (BEM). Among all numerical methods used, BEM seems to gain the most attention from researchers because of its ability to handle complex mathematical formulations, which in this case is the integral of PT itself. For example, Jin et al. (2021) estimate a PT for a cylindrical shape with high conductivity. In their research, BEM was used, and their results show a highly accurate outcome when compared to the analytical solution derived. Other methods used by previous researchers include semi algebraic methods, linear and quadratic element numerical

Authors information:
[a]Department of Mathematical Sciences, Faculty of Science, Universiti Teknologi Malaysia (UTM), Johor Bahru, 81310 Johor, MALAYSIA. E-mail: suzarina@utm.my[1], s.h.yeak@utm.my[2], taufiq@utm.my[3], nurfarrishaasnida@graduate.utm.my[4]

*Corresponding Author: suzarina@utm.my

Received: October 28, 2025
Accepted: May 6, 2026
Published: November 15, 2026

DOI: https://doi.org/10.22452/mjs.vol45sp2.8
Malaysian Journal of Science 45 (Special Issue 2): 74-82 (November 2026)



(a) (b)

Figure 1. (a) T-scan configuration for detection of breast anomaly. (b) Detection of a metal in landmine using metal detector (Ammari and Kang, 2003).

integration, coupling techniques using interpolation and minimization, among others, as seen in works by Khairuddin and Lionheart (2013, 2016), Capdeboscq et al. (2012), Lu et al. (2013), and Sukri et al. (2020). The precision of numerical solutions can vary based on the geometrical shapes used. Various geometries were employed in PT computation, such as benchmarking geometries, spheres and ellipsoids, and other real-life shapes like coins and guns. By applying these methods, researchers aim to understand and improve the effectiveness of PT calculations, especially in real-life applications such as metal detection or similar fields, which can ensure reliable yet efficient outcomes in critical engineering problems.

However, achieving these so-called accurate methods can sometimes incur higher time demands for computation. Since high accuracy is crucial to ensuring that the solution is reliable, the process of obtaining results could make it less practical for real-life applications where rapid and accurate results are critical. The singularity of the PT integral itself makes it challenging to solve analytically, and numerically, it consumes considerable time. To address this issue, this study aims to provide a speed-up technique by implementing geometric modifications as well as exploiting the adaptive properties of PT to ensure that computations are completed in a shorter time while still achieving accurate numerical solutions. By implementing a speeding technique, the computational cost can be optimized in terms of time, enabling computations to be completed faster without sacrificing solution accuracy. These strategies include geometric modifications and adjustments used in PT calculations, which enhance computational efficiency. This study aims to provide a practical solution balancing efficiency and precision for real-life problems where speed and reliability are considered key factors in the methods.

In this paper, we employed a quadratic element integration from a study by Sukri et al. [18], where the speeding up technique is used in the singular integral operator of K_B^* . We perform a comparison of the computation for K_B^* without speeding technique with the new computed singular integral operator K_{BN}^* in terms of its error as well as its execution time. In the next section, we introduce the mathematical background of PT, which is crucial for better insight and understanding of PT, especially first order PT.

2. The second rank polarization tensor

The transmission problem which has been defined by Ammari and Kang (2007), is the origination of the terminology of PT for which a Lipschitz bounded domain called the domain of B is considered where the origin of the domain, O is stated inside B. The conductivity of object is denoted as k which in this case cannot be equivalent to 1 (which is considered to be the same conductivity as the surrounding). The range of the conductivity is from non-negative numbers to infinite numbers $(0 < k \neq 1 \leq +\infty)$. The solution of this transmission problem in equation (1) is denoted as u where H is the harmonic function in $\mathbb{R}^3$.

$$u(x) - H(x) = \sum_{|i|=|j|=1}^{+\infty} \frac{(-1)^{|i|}\partial_x \Gamma(x) M_Q(x_i, y_j)\partial^j H(0)}{i!\, j!}, as\ |x| \to +\infty. \quad (1)$$

In this case, $|i|$ and $|j|$ are multi-indices,$\Gamma(x)$ is the fundamental solution of the Laplacian while $M_Q(x_i, y_j)$ is the first order PT. The definition of the first order PT is represented in terms of an integral equation containing a system of linear equations over the boundary of the domain B which is stated in equation (2).

$$M_Q(x_i, y_j) = \int_{\partial B} y_j \psi_i(y) d\Omega(y)\,, x, y \in \partial B. \quad (2)$$

DOI: https://doi.org/10.22452/mjs.vol45sp2.8
Malaysian Journal of Science 45 (Special Issue 2): 74-82 (November 2026)

The notation for the coordinates for element y is denoted as y_j, while $\psi_i(x)$ is defined as a system of equations as in equation (3).

$$\psi_i(y) = (\lambda I - K_B^*)(N_{V_x}). \quad (3)$$

where $\lambda = 1/2 + 1/(k+1)$ while N_{V_x} is the normal vector of element x with formula $N_{V_x} = V(x).\nabla x_i$. In order to obtain the system of equations, $\psi_i(y)$, we need to solve the singular integral operator K_B^*, where this integral is defined as Cauchy Principle Value integral stated in equation (4).

$$K_B^*\psi(x_i) = \frac{1}{4\pi} P.V. \int_{\partial B} \frac{\langle x_i - y_j, V_{x_i}\rangle}{|x_i - y_j|^3} \psi(y_i) d\Omega(y). \quad (4)$$

where $\psi(x_i) \in \partial B$ such that $L^2(\partial B)$ is a space of square integrable functions. In our study, we aim to focus on the computation of K_B^* whereby the speeding-up technique is applied to this integral. The reason the integral is chosen is that when we referred to the study by Sukri et al. (2020), it is observed that the matrix that is formed as Gaussian quadrature is implemented using to a symmetric matrix. Hence, instead of calculating the whole matrix, we only calculate the upper or lower part of the matrix and multiply it by two. It seems that the process is simple. However, in order to define the geometry in Netgen Mesh Generator, which is the meshing software used to discretize the geometry, we need to define a hollow object, where, in this case, we only consider the boundary of the element. After we implemented the speeding process, we compared the numerical solutions in terms of reduction time percentage as well as its relative error. As mentioned in the study by Ammari and Kang (2007), we refer to the following theorem which can validate the result and the numerical solutions that have been computed.

2.1 Theorem and Proving

Theorem 1 The matrix 3×3 of the first order polarization tensor is symmetric and positive definite if the conductivity of the object inclusion is more than 1, while negative definite if the conductivity is between 0 and 1.

Theorem 1 has been proven by Khairuddin et al. (2013) where the researchers separate the proof involving ellipsoid object inclusion $x^2/a^2 + y^2/b^2 + z^2/c^2 = 1$ into two parts:

[1] Matrix of the first order PT, $M(k, B)$ is positive definite matrix if and only if $k > 1$;

[2] Matrix of the first order PT, $M(k, B)$ is positive definite matrix if and only if $k < 1$.

Proof For part [1], the researchers assume $k > 1$ and $M(k, B)$ is the first-order PT for the ellipsoid. Then, the matrix of PT is represented as

$$M(k,B) = (k-1)|B| \begin{bmatrix} M_1 & 0 & 0 \\ 0 & M_2 & 0 \\ 0 & 0 & M_3 \end{bmatrix}.$$

Let $\alpha_i = (k-1)|B|M_i$ for $i = 1,2$ and 3. The conductivity $k > 1$ since $k - 1 > 0$ and clearly $|B| > 0$ as well as $M_i > 0$ which satisfies Proposition 1 with $0 < k \neq 1 < +\infty$.

Proposition 1 The depolarization factors, D_i for $i = 1,2,3$ satisfies $0 < D_1 < 1$

$\alpha_i > 0$, which is the diagonal of matrix $M(k, B)$ and $M(k, B)$, is a positive definite matrix. Next, assume $M(k, B)$ is a positive definite matrix. We need to show $k > 1$.

$$M(k,B) = (k-1)|B| \begin{bmatrix} M_1 & 0 & 0 \\ 0 & M_2 & 0 \\ 0 & 0 & M_3 \end{bmatrix}.$$

Let $\alpha_i = (k-1)|B|M_i$ for $i = 1,2$ and 3. Since $M(k, B)$ is a positive definite matrix, then the eigenvalues, $\alpha_i > 0$. Here, $|B| > 0$. Since $0 < k \neq 1 < +\infty$ and $0 < D_1 < 1$ based on Proposition 1, $M_i > 0$. For $\alpha_i > 0$, $(k-1) > 0$ and we can conclude that $k > 1$.

For part [2], assume $k < 1$. We need to show the $M(k, B)$ is negative definite matrix. Using the same approach, we let $M(k, B)$ be the first order PT for ellipsoid. Then, the matrix of PT is represented as

$$M(k,B) = (k-1)|B| \begin{bmatrix} M_1 & 0 & 0 \\ 0 & M_2 & 0 \\ 0 & 0 & M_3 \end{bmatrix}.$$

Let $\alpha_i = (k-1)|B|M_i$ for $i = 1,2$ and 3. The conductivity $k < 1$, then $k - 1 < 0$, and clearly $|B| > 0$, as well as $M_i > 0$, which satisfies Proposition 1 with $0 < k \neq 1 < +\infty$. $\alpha_i > 0$, which is the diagonal of matrix $M(k, B)$ and it conclude that $M(k, B)$ is a negative definite matrix. Next, assume $M(k, B)$ is a positive definite matrix. We need to show $k < 1$.

$$M(k,B) = (k-1)|B| \begin{bmatrix} M_1 & 0 & 0 \\ 0 & M_2 & 0 \\ 0 & 0 & M_3 \end{bmatrix}.$$

Let $\alpha_i = (k-1)|B|M_i$ for $i = 1,2$ and 3. Since $M(k, B)$ is a positive definite matrix, then the eigenvalues, $\alpha_i > 0$. Here, $|B| > 0$. Since $0 < k \neq 1 < +\infty$ and $0 < D_1 < 1$ based on Proposition 1, $M_i > 0$. For $\alpha_i > 0$, $(k-1) < 0$, we can conclude that $k < 1$. In the next section, the analytical solution was derived by Ammari and Kang [2], and is represented where the analytical solution was used as a benchmark. Different notations of $M(k, B)$ were used in order to differentiate between the analytical solution M_A and the approximated solution M_E.

2.2 The Analytical Solutions of the Second Rank Polarization Tensor for Sphere and Ellipsoid

The derived analytical solution provided by Ammari and Kang (2007) is based on the ellipsoid with radius 1. First, the researchers consider an ellipsoid with the general equation $x^2/A + y^2/B + z^2/C = 1$. The condition for the semi principal axes A, B and C is $0 < C = B = A$. The analytical solution of the ellipsoid is represented by a 3×3 matrix for which the main

DOI: https://doi.org/10.22452/mjs.vol45sp2.8
Malaysian Journal of Science 45 (Special Issue 2): 74-82 (November 2026)

diagonal is in integral form containing the semi principal axes A, B and C as represented in the following equation.

$$M_A(x_i, y_j)|_{(k,Ellipsoid)} = \frac{4\pi\varphi(A \cdot B \cdot C)}{3} \begin{bmatrix} \frac{1}{1+D_1\varphi} & 0 & 0 \\ 0 & \frac{1}{1+D_2\varphi} & 0 \\ 0 & 0 & \frac{1}{1+D_3\varphi} \end{bmatrix}. \quad (5)$$

where $\varphi = k - 1$ while D_1, D_2 and D_3 are in the form of an integral containing the semi principle axes of A, B and C, given as

$$D_1 = \int_1^{+\infty} \frac{B \cdot C}{t^2\sqrt{(A^2(t^2-1)+B^2)}\sqrt{A^2(t^2-1)+C^2}} dt,$$
$$D_2 = \int_1^{+\infty} \frac{B \cdot C}{\sqrt{(A^2(t^2-1)+B^2)}\left(t^2-1+\left(\frac{B}{A}\right)^2\right)^2\sqrt{A^2(t^2-1)+C^2}} dt, \quad (6)$$
$$D_3 = \int_1^{+\infty} \frac{B \cdot C}{\sqrt{(A^2(t^2-1)+B^2)}\left(t^2-1+\left(\frac{C}{A}\right)^2\right)^2\sqrt{A^2(t^2-1)+C^2}} dt.$$

To obtain the analytical solution for a sphere, we ensure that the semi principal axes are equal to each other $A = B = C$. By setting semi-principal axes to become equal to each other, the integral for D_1, D_2 and D_3 yield to $1/3$. Hence, the resulting first order PT for a sphere can be computed using the following formula

$$M_A(x_i, y_j)|_{(k,Sphere)} = \frac{4\pi\varphi r^2}{3} \begin{bmatrix} \frac{1}{1+\frac{1}{3}\varphi} & 0 & 0 \\ 0 & \frac{1}{1+\frac{1}{3}\varphi} & 0 \\ 0 & 0 & \frac{1}{1+\frac{1}{3}\varphi} \end{bmatrix}. \quad (7)$$

From the integral of PT in (2), we implement the previous method by Sukri et al. (2020), together with the acceleration techniques which are applied to equation (4), and then compare them with the analytical solution in equations (5) and (7). In this study, we employ a symmetrical geometry with known analytical solutions specifically a sphere, to ensure that our technique are both reliable and effective in terms of accuracy.

3. Speeding up techniques using adaptive geometrical modification

3.1 Netgen Mesh Generator (NG Solve version 6.2)

We start the speeding technique by discretizing a hemisphere into triangular meshes in a meshing software called Netgen Mesh Generator. It is a user-friendly software developed by Joachim Schöberl (1997) that can generate both triangular and quadrilateral meshes for two-dimensional and three-dimensional objects. However, despite its advantages, there is a limitation to this software, as users cannot set the desired number of meshes. The flowchart shown in Figure 2 represents the process of discretizing an object using Netgen Mesh Generator. The flowchart illustrates the steps involved, starting from the initialization of geometry and ending with the final generation of meshes for the geometry.

However, not every geometric shape is provided by the software developer within the application. Other shapes, such as a hemisphere, are not defined in Netgen Mesh Generator. Therefore, if we want a specific shape, we need to define it first using another programming language, which is Python. Due to its compatibility with Netgen Mesh Generator software, we can directly import the predefined shape into Netgen Mesh Generator for mesh generation purposes. In this case, we create a hemisphere with an open bottom, as illustrated in Figure 3. The reason a hemisphere was chosen is that we aim to duplicate it to become a sphere and then calculate its PT while comparing it with the given analytical solution. These steps allow users to customize their own geometry, which can be complicated or complex geometries.

Based on Figure 3, as we duplicate the upper part of the hemisphere, it is observed that there is redundancy in the number of nodes at the axis of symmetry where in this case our axis of symmetry is at $z = 0$. The redundancy of the nodes can make the mesh structure more complex and increase the potential for inaccurate computation and analysis. To address this, several techniques must be employed to remove the redundant nodes. This technique involves removing, redefining and renumbering the nodes accordingly. After successfully defining the new nodes, surface elements and meshes, the computation of the singular integral operator of PT, K_{BN}^* can be carried out. From the properties of matrix of K_B^*, we categorize the computation into three cases.

4. Cauchy principle valiue integral of polarization tensor

The computation of the PT is based on these cases. In order to avoid repetitive computation of the normal vector, V_{x_i}, the computation of a singular integral operator is calculated separately from the original equation of K_B^* and is stored in pre-allocated memory in Matlab. This is to ensure that, minimal memory is used to compute the CPV integral. The integral of the CPV now is expressed as

$$K_B^*\psi(x_i) = \frac{1}{4\pi} P.V. \int_{\partial B} \frac{\langle x_i - y_j \rangle}{|x_i - y_j|^3} \psi(y_i) d\Omega(y). \quad (8)$$

DOI: https://doi.org/10.22452/mjs.vol45sp2.8
Malaysian Journal of Science 45 (Special Issue 2): 74-82 (November 2026)

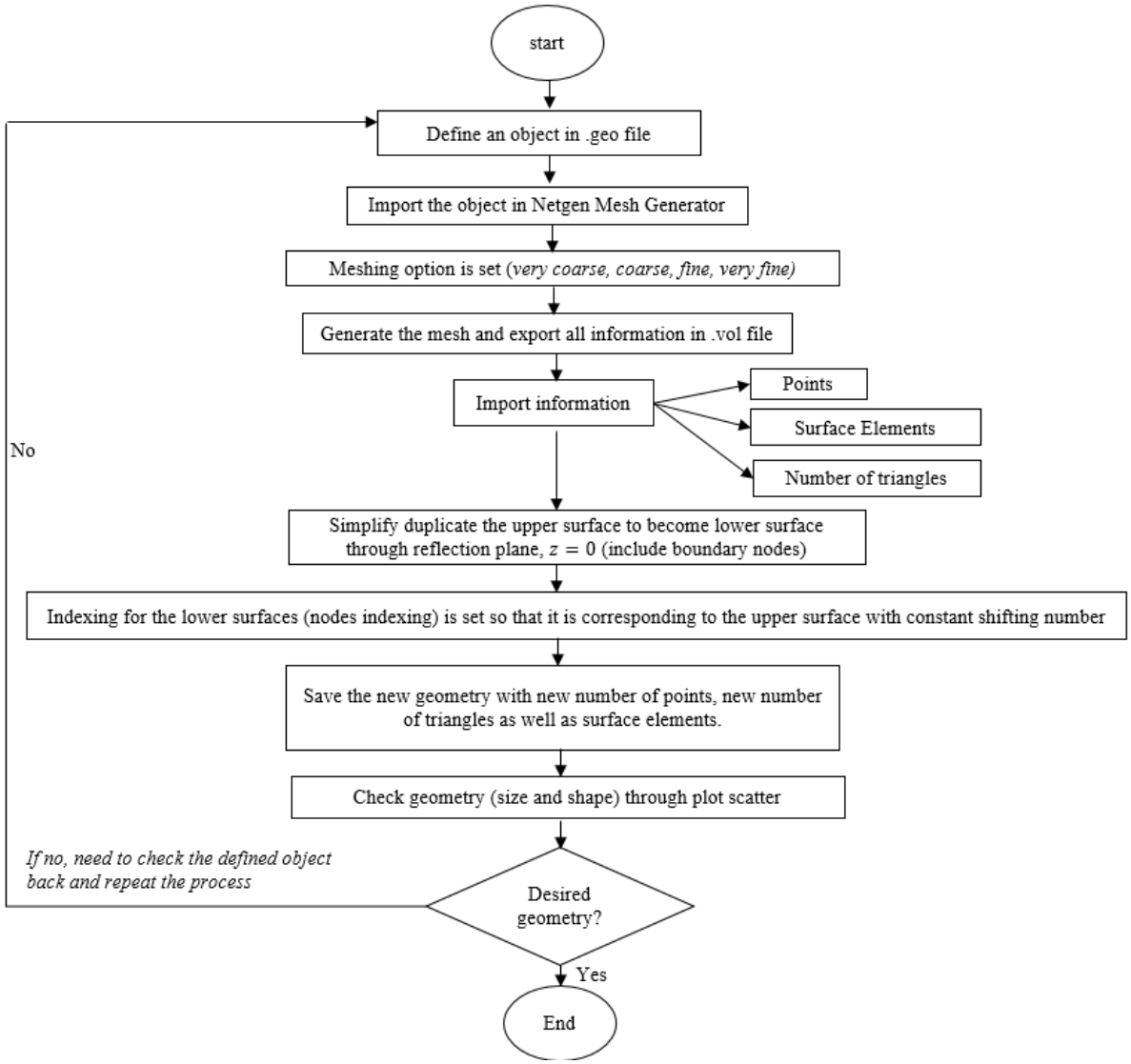
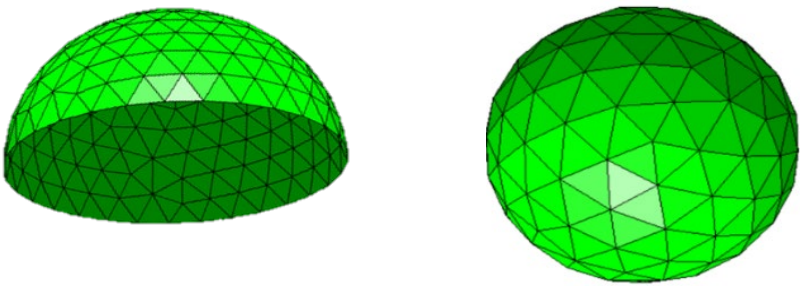


Figure 2. Flow chart illustrating the process to create a sphere from a hemisphere.



(a) (b)

Figure 3. (a) A hemisphere with open bottom is discretized into 359 meshes with radius 3. (b) Duplication of a hemisphere with open bottom to become a sphere with 718 meshes with radius 3.

DOI: https://doi.org/10.22452/mjs.vol45sp2.8
Malaysian Journal of Science 45 (Special Issue 2): 74-82 (November 2026)

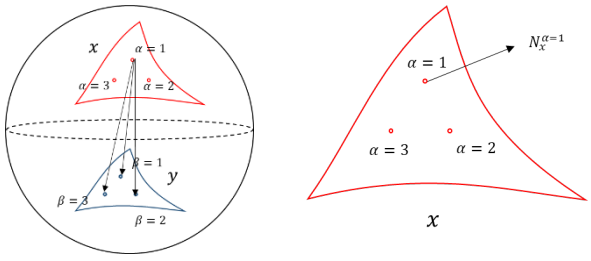
In this case, $x - y$ is the difference between elements within the geometry which is expressed in terms of the distance between the Gaussian points in each element as

$$x_{N_x}^{\alpha=1} - y_{N_y}^{\alpha=1,2,3} = \begin{bmatrix} x_{N_x}^{\alpha=1} - y_{N_y}^{\alpha=1} \\ x_{N_x}^{\alpha=1} - y_{N_y}^{\alpha=2} \\ x_{N_x}^{\alpha=1} - y_{N_y}^{\alpha=,3} \end{bmatrix},$$
$$x_{N_x}^{\alpha=2} - y_{N_y}^{\alpha=1,2,3} = \begin{bmatrix} x_{N_x}^{\alpha=2} - y_{N_y}^{\alpha=1} \\ x_{N_x}^{\alpha=2} - y_{N_y}^{\alpha=2} \\ x_{N_x}^{\alpha=2} - y_{N_y}^{\alpha=,3} \end{bmatrix}, \quad (9)$$
$$x_{N_x}^{\alpha=3} - y_{N_y}^{\alpha=1,2,3} = \begin{bmatrix} x_{N_x}^{\alpha=3} - y_{N_y}^{\alpha=1} \\ x_{N_x}^{\alpha=3} - y_{N_y}^{\alpha=2} \\ x_{N_x}^{\alpha=3} - y_{N_y}^{\alpha=,3} \end{bmatrix}.$$

where N_x and N_y are the number of surface elements. The normal vector for the element x is expressed as

$$V_{x_{N_x}}^{\alpha=1,2,3} = \begin{bmatrix} V_{x_{N_x=1}}^{\alpha=1,2,3} \\ \vdots \\ V_{x_{N_x=N}}^{\alpha=1,2,3} \end{bmatrix}, \quad (10)$$

In this paper, we focus on a sphere with radius 3, as illustrated in Figure 4 a), while the normal vector for element x, V_x for three Gaussian points, $\alpha = 1,2$ and 3, is illustrated in Figure 4 b).



(a) (b)

Figure 4. a) The distance between element x and element y for a sphere with radius 3 b) Normal vector for element x, V_x.

The integral of CPV yields a matrix of $3N_x \times 3yN_x$. It is observed that the upper triangular matrix generates the same values for the lower triangular matrix of K_{BN}^*. Therefore, instead of computing all elements of the matrix, we categorize the matrix according to six cases in total. In this case, we can minimize the time taken for the computation of K_{BN}^* without neglecting its accuracy.

$$\begin{aligned}
Case\ (i) \rightarrow K_{BN}^*([i,gp],[i+N_{el},gp]) &= \langle -1,-1,-1\rangle \\ &\cdot K_{BN}^*([i+N_{el},gp],[i,gp]), \\
Case\ (iia) \rightarrow K_{BN}^*([i,gp],[j+N_{el},gp]) &= \langle 1,1,-1\rangle \\ &\cdot K_{BN}^*([i+N_{el},gp],[j,gp]), \\
Case\ (iib) \rightarrow K_{BN}^*([j+N_{el},gp],[i,gp]) &= \langle 1,1,-1\rangle \\ &\cdot K_{BN}^*([j,gp],[i+N_{el},gp]), \\
Case\ (iiia) \rightarrow K_{BN}^*([i,gp],[j,gp]) &= \langle -1,-1,-1\rangle \\ &\cdot K_{BN}^*([i+N_{el},gp],[j \\ &+N_{el},gp]), \\
Case\ (iiib) \rightarrow K_{BN}^*([j,gp],[i,gp]) &= \langle -1,-1,-1\rangle \\ &\cdot K_{BN}^*([j+N_{el},gp],[i \\ &+N_{el},gp]),
\end{aligned} \quad (11)$$

From equation (11), i and j are the indexing of the elements x and y, are the number of surface elements for the upper part of the sphere. gp is the Gaussian point of three point Gaussian quadrature, which is expressed in shape functions, $N_k(\xi,\eta)$ in terms of ξ and η where $k = 1,2,3,4,5$ and 6, as

$$\begin{aligned}
N_1 = 2\xi^2 - \xi, N_2 = 2\eta^2 - \eta, N_3 &= 2\xi^2 + 2\eta^2 + 4\xi\eta - \xi - \eta \\ &+ 1, \\
N_4 = 4\xi\eta, N_5 = -4\eta^2 - 4\xi\eta + 4\eta, N_6 &= -4\xi^2 - 4\xi\eta + 4\eta.
\end{aligned} \quad (12)$$

Instead of computing the matrix of K_{BN}^* as a whole, we compute the matrix by cases. Then time reduction is observed. Although it seems that, many modifications are needed in order to complete the matrix computation, it is observed that the time reduction is significant. The percentage of time reduction is calculated using the formula in equation (13).

$$Time\ reduction = \frac{Time\ \ to\ execute\ (Duplicated\ N)}{Time\ to\ execute\ (N\ without\ duplication)} \times 100\% \quad (13)$$

Based on the modification of the geometry, it is observed that the total time reduction percentage can be as low as 12%. However, some external factors that we cannot control, such as the processor running in the background of MATLAB and memory handling, can cause the reduction time percentage to vary for each duplication of elements. After completing the speeding technique, we compare the relative error in equation (14) for the second-rank PT, where we must ensure that the technique does not affect the computation of the PT itself.

DOI: https://doi.org/10.22452/mjs.vol45sp2.8
Malaysian Journal of Science 45 (Special Issue 2): 74-82 (November 2026)

$$Relative\ Error = \frac{|M_E - M_A|}{|M_E|}. \quad (14)$$

M_E is the exact solution for second rank PT while M_A is the computed second rank PT based on the speeding technique and without the speeding technique. In the next section, numerical examples based on a sphere with radius 3 and conductivity, is $k = 1.5$ are computed and the time reduction is recorded.

5. Numerical examples of second rank polarization tensor

5.1 Comparative Analysis of the Execution Time for K_B^* and K_{BN}^*

This section presents an analysis of the execution time to compute the CPV integral with and without speeding technique. The performance of the numerical computation is observed based on the time taken for the numerical computation to finish. However, we must take account other factors that may influence the time of execution. Computing the CPV integral can be computationally intensive due to the singularity of the integral itself. A comparative study is conducted, where we compare the time execution , K_{BN}^* with speeding technique, K_B^* for different numbers of surface elements. In order to perform the comparative analysis, the mesh size or number of surface elements for a sphere is generated using Netgen Mesh Generator. However, the mesh size cannot be set according to the user's preference. Therefore, for the numerical computation for K_B^*, the number of surface elements that is obtained from the software is $N = 28, 42, 130, 278, 354, 714$ and 2842 meshes, while the time to compute it is recorded in Table 1.

Table 1. Time to execute the numerical computation for K_B^* of a sphere with radius 3 and conductivity, $k = 1.5$.

Mesh size, N	Time to execute K_B^* (second)
28	0.812500
42	1.718750
130	15.46875
278	68.8750
354	113.03125
718	571.96875
2842	7390.203125

Table 2. Time to execute the numerical computation for K_{BN}^* of a sphere with radius 3 and conductivity, $k = 1.5$.

Mesh size, N	Time to execute K_{BN}^* (second)
28	0.578125
42	1.406250
116	12.593750
280	58.312500
464	94.406250
652	396.125000
2608	6474.515625

Meanwhile, for the computation of the new K_{BN}^*, instead of generating a full sphere, as described in the previous section, we generate a hemisphere with the same radius as the sphere generated in Table 1. As a result, the mesh size is effectively half of the resulting mesh described in Table 2. We generate multiple mesh sizes and then duplicate the hemisphere to form a complete sphere (while ensuring that the boundaries at $z = 0$ do not overlap). This allows us to match the mesh size in Table 1, ensuring fair comparison between K_{BN}^* and K_B^* .

Table 1 and Table 2 depicts the time for execution for the CPV integral both with and without geometry modification. By comparing the results from the Table, the numerical computation for the new K_{BN}^* is lower than K_B^* as the number of mesh increases. This suggests that the computation using the geometry modification is more optimized and less complex than the original computation of the CPV integral.

Table 3 shows the percentage of time reduction calculated using equation (13). A reduction in computation time for the CPV integral with a radius of 3 and conductivity $k = 1.5$, across tested mesh sizes is depicted as a range of approximately 12% to 30% time reduction. This indicates that the geometry modification leads to a reduction in computation time. However, the time reduction depends on the mesh size, whereas, the highest performance of 30.74% occurs at mesh size 718 (after duplication) while the lowest performance can be seen at mesh size 2842, with performance 13.29. External factors such as background processes, memory availability as well as operating system overhead may influence the time reduction percentage. It is observed that, as the number of surface elements increases, the time to execute is increases. This is due to the size of the matrix computation in the CPV integral itself.

Table 3. Percentage of time reduction to execute the numerical computation for the new sphere with radius 3 and conductivity, $k = 1.5$.

Mesh Size, N (before duplication)	Mesh Size, N (after duplication)	Percentage of time reduction $(\%)$ for K_{BN}^*
14	28	28.85
21	42	18.18
65	130	18.59
139	278	15.34
177	354	16.48
359	718	30.74
1421	2842	12.39

Figure 5 depicts the difference between the execution time for the computation of K_{BN}^* and K_B^*. From the figure, we observe that as the number of elements increases, the computation increases. This is due to the increasing size of the matrix of the CPV integral. As the matrix size increases, computational resources such as memory and processing power also increase. This leads to a longer computation time for the singular integral of the CPV integral as reflected in Figure 5, where both execution time for K_{BN}^* and K_B^* is increase as the number of surface elements increases. Larger matrix sizes can pose challenge in

DOI: https://doi.org/10.22452/mjs.vol45sp2.8
Malaysian Journal of Science 45 (Special Issue 2): 74-82 (November 2026)

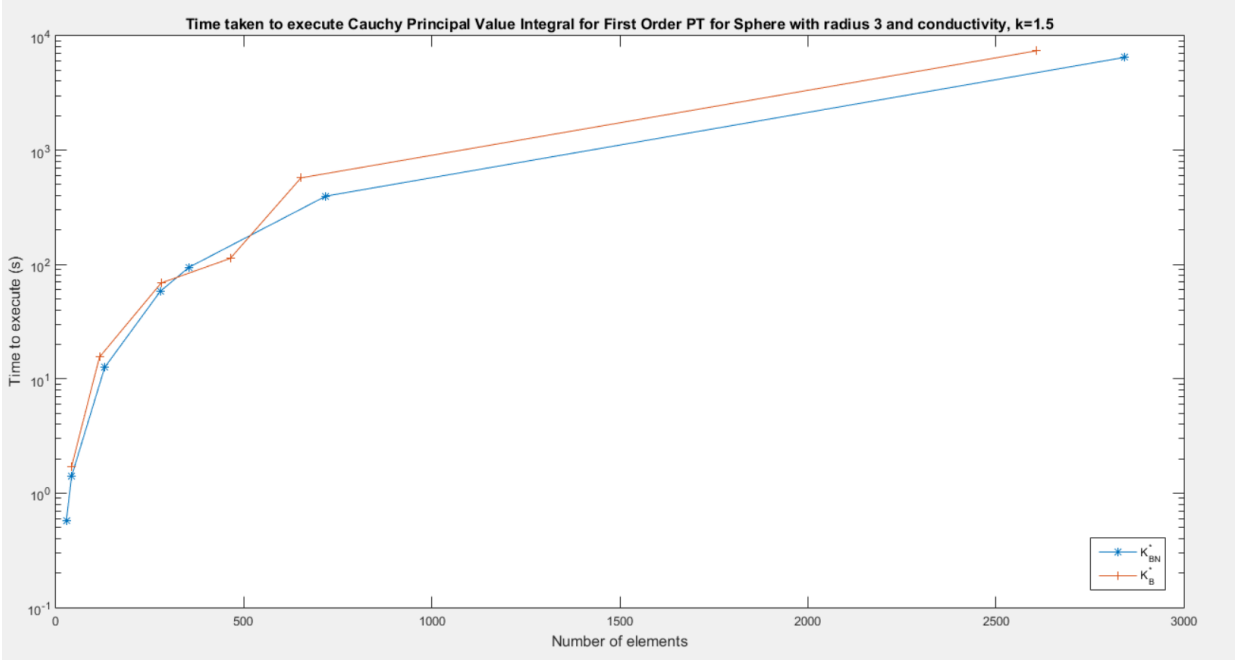


Figure 5. Execution time for K^*_{BN}(with speeding) and K^*_B(without speeding) for the first order PT calculation on a sphere with radius 3, conductivity, $k = 1.5$ and the number of surface elements for $N^* = 28, 48, 130, 278, 354, 718,$ and 2842 while $N = 42, 116, 280, 464, 652$ and 2608.

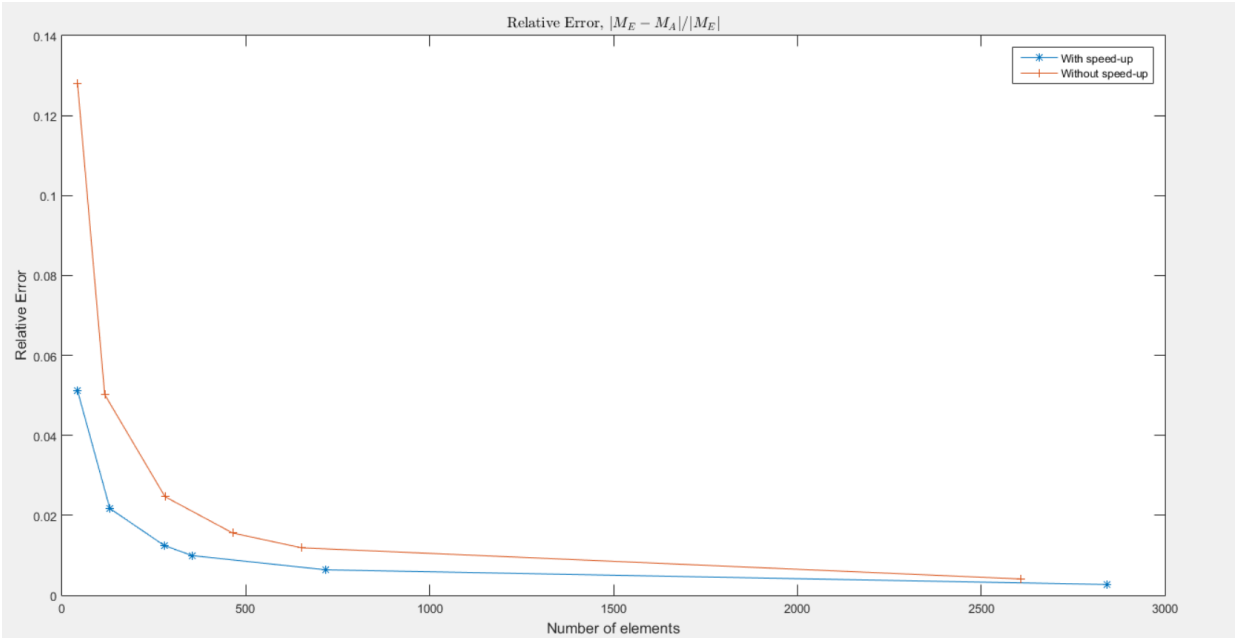


Figure 6. Convergence of the relative error using for the first order PT calculation on a sphere with radius 3, conductivity, $k = 1.5$ and the number of surface elements for $N^* = 28, 48, 130, 278, 354, 718,$ and 2842 while $N = 42, 116, 280, 464, 652$ and 2608.

numerical stability. The stability of a larger matrix size is critical and often has a higher sensitivity to perturbations where, any changes or perturbations can make the matrix ill-conditioned, thus rendering it unstable. Hence, computation by cases, as mentioned in equation (11), is required, which can lead to a lower relative error for the entire process of obtaining the second rank PT, as observed in Figure 6. From Figure 6, the computed relative error using equation (14) shows that the relative error for the second rank PT with the speeding technique applied is lower than the relative error without the speeding technique.

DOI: https://doi.org/10.22452/mjs.vol45sp2.8
Malaysian Journal of Science 45 (Special Issue 2): 74-82 (November 2026)

6. Conclusion

In conclusion, this paper has demonstrated the effectiveness of the speeding technique for tackling high singularity integrals, as shown in the integral of PT. The techniques proposed are easy to implement and can be applied to symmetrical object inclusion, where this technique not only reduces computation time but also has proven effective in real-life problems where faster computation is essential. By addressing the challenges associated with higher singularities in the mathematical computation of PT, we have shown that it is possible to achieve accurate numerical solutions while significantly reducing computation time. The integration of advanced numerical techniques, alongside adaptive mesh refinement, has been instrumental in enhancing both speed and precision. The results indicate that our approach meets the demands of complex systems and offers practical solutions for engineering applications where computational efficiency is important. The implementation of adaptive geometrical modifications, enabled by the Netgen Mesh Generator, further emphasizes the potential of these techniques in optimizing computational processes. Overall, this study contributes valuable insights into the intersection of numerical methods and engineering practices, paving the way for future research and applications in the field. The advancements outlined herein not only improve current methodologies but also lay a foundation for continued exploration of more efficient computational techniques.

7. Acknowledgement

The authors would like to acknowledge the financial support from Universiti Teknologi Malaysia (UTM) for the financial funding under the UTM Encouragement Research (UTMER) grant scheme with reference number PY/2024/00856 and cost center number Q.J130000.3854.42J43.

8. References

Alkhalifah, T. A. "Efficient computation of polarization tensors for the detection of buried landmines." Journal of Applied Geophysics, 107 (2014): 74-81.

Ammari, H., and Kang, H., “Properties of the generalized polarization tensors,” *Multiscale Model. Simul.* 1, 335–348 (2003).

Ammari, H., and Kang, H., *Polarization and moment tensors: with applications to inverse problems and effective medium theory*, Vol. 162 (Springer Science & Business Media, 2007).

Bannister, J. R., and Gupta, V. "Electromagnetic detection of buried objects using the polarization tensor." Journal of Geophysical Research, 114 (2009): B12202.

Bardet, J. P., and Vasseur, J. "Generalized polarization tensors in the study of magnetically induced currents." Journal of Applied Physics, 97(10) (2005): 10C102.

Capdeboscq, Y., Karrman, A. B., and Nedelec, J. C., “Numerical computation of approximate generalized polarization tensors,” *Appl. Anal.* 91, 1189-203 (2012).

de Jong, W., Cremer, F., Schutte, K., and Storm, J., “Usage of polarization features of land mines for improved automatic detection,” in *Detection and Remediation Technologies for Mines and Minelike Targets V*, Vol. 4038, 241-252 (SPIE, 2000).

Friedman, A., and Vogelius, M., “Identification of small inhomogeneities of extreme conductivity by boundary measurements: a theorem on continuous dependence,” *Arch. Rational Mech. Anal.* 105, 299-326 (1989).

Jin, Zhongwen, Ganghua Qin, Haidong Fan, Ruochen Huang, Ziqi Chen, Qian Zhao, Mingyang Lu, Zhijie Zhang, Anthony Peyton, and Wuliang Yin. "Boundary-element analysis of magnetic polarization tensor for metallic cylinder." IEEE Access 9 (2021): 63250-63256.

Lu, Zhijie Zhang, Anthony Peyton, and Wuliang Yin. "Boundary-element analysis of magnetic polarization tensor for metallic cylinder." IEEE Access 9 (2021): 63250-63256.

Kang, H., and Ammari, H. "Generalized polarization tensors and their applications." Inverse Problems, 22(1) (2006): 305-317.

Khairuddin, T. K. A., and Lionheart, W., “Some properties of the first order polarization tensor for 3-D domains,” *Matematika* 19, 1-18 (2013).

Khairuddin, T. K. A., and Lionheart, W. R., “Computing the first order polarization tensor: welcome BEM++!,” *Menemui Matematik* 35, 15-20 (2013).

Khairuddin, T. K. A., and Lionheart, W. R., “Characterization of objects by electrosensing fish based on the first order polarization tensor,” *Bioinspir. Biomim.* 11, 055004 (2016).

Lu, M., Zhao, Q., Hu, P., Yin, W., and Peyton, A. J., “Prediction of the asymptotical magnetic polarization tensors for cylindrical samples using the boundary element method,” in *2015 IEEE Sensors Applications Symposium (SAS)*, 1-4 (IEEE, 2015).

Pólya, G., “A minimum problem about the motion of a solid through a fluid,” *Proc. Natl. Acad. Sci.* 33, 218-221 (1947).

Roux, M., and Gloaguen, R. "Application of generalized polarization tensors to electromagnetic modeling of complex geological structures." Geophysical Journal International, 205(3) (2016): 1836-1855.

S. A. Sukri, Y. S. Hoe, and T. K. A. Khairuddin, “Quadratic element integration of approximated First Order Polarization Tensor for sphere,” Malaysian J. Fundam. Appl. Sci. 16(5), 560–565 (2020).

Schöberl, Joachim. "NETGEN An advancing front 2D/3D-mesh generator based on abstract rules." Computing and visualization in science 1, no. 1 (1997): 41-52.

DOI: https://doi.org/10.22452/mjs.vol45sp2.8
Malaysian Journal of Science 45 (Special Issue 2): 74-82 (November 2026)